

Near-Infrared Spectroscopy of Very Low-Luminosity Young Stellar Objects in the Taurus Molecular Cloud

Yoichi ITOH

Graduate School of Science and Technology, Kobe University, 1-1 Rokkodai, Nada, Kobe, Hyogo 657-8501

yitoh@kobe-u.ac.jp

Motohide TAMURA

National Astronomical Observatory of Japan, 2-21-1 Osawa, Mitaka, Tokyo 181-8588

tamuramt@cc.nao.ac.jp

and

Alan T. TOKUNAGA

Institute for Astronomy, University of Hawaii 2680 Woodlawn Drive, Honolulu, Hawaii 96822, USA

tokunaga@ifa.hawaii.edu

(Received 2000 December 31; accepted 2001 January 1)

Abstract

We have carried out near-infrared spectroscopic observations of 23 very low-luminosity young stellar object (YSO) candidates and 5 their companions in Heiles Cloud 2, one of the densest parts of the Taurus molecular cloud. Twelve objects were confirmed as YSOs by Br γ feature. The effective temperatures of the YSOs and of the companions are estimated from the 2.26 μm feature, the 2.21 μm feature, and the H $_2$ O band strengths. Detailed comparisons of our photometric and spectroscopic observations with evolutionary tracks on the HR diagram suggest some objects to be very low-mass YSOs.

Key words: stars: formation — stars: low-mass stars, brown dwarf — infrared: stars

1. Introduction

Recent optical and near-infrared photometric studies have revealed faint populations of young stellar object (YSO) candidates in low-mass star forming regions (000 [cite]cite.ComeronComeron et al.(1993); 000 [cite]cite.Strom95Strom et al.(1995); 000 [cite]cite.ITGItoh et al.(1996), hereafter ITG; 000 [cite]cite.BarsonyBarsony et al.(1997); 000 [cite]cite.Oasa99Oasa et al.(1999)), in intermediate-mass star forming regions (000 [cite]cite.AspinAspin et al.(1994)), and even in high-mass star forming regions (000 [cite]cite.KaifuKaifu et al.(2000); 000 [cite]cite.Lucas00Lucas & Roche(2000); 000 [cite]cite.Oasa02Oasa et al(2002)). Their faintness is suggestive of low-mass; they may be very low-mass young stars near the stellar/substellar boundary, young brown dwarfs, or even free floating planets.

From the photometric observations alone, however, it is impossible to simultaneously determine the mass and age of a YSO. Near-infrared spectroscopy of YSO candidates is necessary to overcome this difficulty (000 [cite]cite.Greene95Greene & Meyer(1995); 000 [cite]cite.Luhman97Luhman et al.(1997); 000 [cite]cite.LuhmanRiekeLuhman & Rieke(1998); 000 [cite]cite.Luhman98Luhman et al.(1998); 000 [cite]cite.WilkingWilking et al.(1999); 000 [cite]cite.CushingCushing et al.(2000); 000 [cite]cite.Lucas01Lucas et al.(2001)). Spectra of some faint YSO candidates exhibit the absorption features distinctive to late spectral type, implying young brown

dwarfs. While such very low-mass objects may be ubiquitous in star-forming regions, detail of the formation process of such objects, for example mass function, object density, and disk property, is still unknown.

[cite]cite.Briceno98Briceno (1998) ([cite]cite.Briceno98Briceno (1998)) have carried out an optical search for very low-mass YSOs in the L1495, L1529, L1551, and B209 regions in the Taurus molecular cloud. From photometry with spectroscopy, they found 9 new YSOs in the clouds, half of them have very late spectral types, implying very low-mass objects (0.05 M_{\odot} – 0.25 M_{\odot}). [cite]cite.Luhman00Luhman(2000) ([cite]cite.Luhman00Luhman(2000)) further investigated very low-mass YSOs in the same clouds by combining optical imaging with near-infrared spectroscopy. They found that the mass function of the YSOs in these regions has a peak at 0.8 M_{\odot} and is relatively flat between 0.1 M_{\odot} and 0.8 M_{\odot} range. In these papers, however, because the targets for the spectroscopy were fully or partially selected based on the optical color-magnitude diagram, the sample may not be complete especially for embedded very low-mass objects.

ITG conducted a near-infrared survey of the central $1^{\circ} \times 1^{\circ}$ region of Heiles Cloud 2 in the Taurus molecular cloud, one of the best-studied low-mass star forming regions, with a limiting magnitude of 13.4 mag in the K -band. Fifty YSO candidates were identified by their intrinsic red color on the ($J - H$, $H - K$) color-color diagram, following the scheme discussed by [cite]cite.Strom93Strom et al.(1993) ([cite]cite.Strom93Strom et al.(1993)). Successive high-resolution imaging survey discovered 5 companion candidates around the YSO candidates

(000 [cite]cite.ITNItoh et al.(1999)). Faintness of some YSOs and their companion may be an indicative of the low-mass of the objects.

We describe here near-infrared spectroscopic follow-up of these faint YSO candidates in the Heiles Cloud 2. The observations are described in §2, and data reduction procedures in §3. In §4, we derive effective temperatures of the YSOs mainly from the $2.21 \mu\text{m}$ feature, the $2.26 \mu\text{m}$ feature, and the H_2O absorption band. We also calculate photospheric luminosity of the YSOs from the previous photometry, then plot the YSOs on the HR diagram.

2. Observations

2.1. UKIRT observations

Twenty-one YSO candidates were selected for the spectroscopic observations (table 1). The sample is nearly flux-limited; The K -band magnitudes range from 8 to 12, up to 4 mag fainter than that of classical T Tauri Stars (CTTSs) in the Taurus molecular cloud. We missed ITG 8 and ITG 34 probably due to errors in the coordinates. As template stars, 3 late-type CTTSs, 1 class I source, and 7 late-type dwarfs were also observed.

Spectroscopic observations have been carried out during 1996 November 24 – 26 using the UK Infrared Telescope (UKIRT) at the summit of Mauna Kea, with the Cooled Grating Spectrometer 4 (CGS4, 000 [cite]cite.MountainMountain et al.(1991)). CGS4 has a 256×256 InSb array with a spatial scale of $1.''22 \text{ pixel}^{-1}$. The 75 line mm^{-1} grating was used with the $1.''2$ slit, providing wavelength coverage of $1.8 \mu\text{m} - 2.5 \mu\text{m}$ with resolution $R(= \lambda/\Delta\lambda)$ of 300 at $2.21 \mu\text{m}$. The integration time used for each source was typically 1 – 20 seconds depending on source brightness. In most cases, 96 exposures were taken for each object. Nodding of the telescope was carried out approximately 16 arcsec along the slit for sky subtraction. For the YSO candidates and CTTSs, SAO 76542 (A2V) was observed for correction of the effects of telluric absorption. For late-type dwarfs, we observed stars with spectral types of A0V – A3V at similar airmass. Exposures of an incandescent lamp on and off were taken at the start of each night as dome flats. Exposures of a krypton lamp were taken every three or four hours for wavelength calibrations.

2.2. Subaru observations

The observed objects are 5 binary candidates listed in [cite]cite.ITNItoh et al.(1999) ([cite]cite.ITNItoh et al.(1999)) (table 1). The K -band magnitudes of the companions range from 13 to 16. Six late-type dwarfs were also observed as templates, among which 3 latest dwarfs were observed both with UKIRT and Subaru.

Spectroscopic observations have been carried out on 2000 December 4 – 5 with the Infrared Camera and Spectrograph (IRCS, 000 [cite]cite.Tokunaga98Tokunaga et al.(1998); 000 [cite]cite.KobayashiKobayashi et al.(2000)) on the Subaru Telescope at the summit of Mauna Kea, Hawaii. IRCS has a 1024×1024 InSb array with spatial scale of $0.''058 \text{ pixel}^{-1}$. Typical seeing size

was $0.''4$ with a stable condition for both observing dates, so that all binaries were well separated. The grating provided a wavelength coverage of $2.0 \mu\text{m} - 2.5 \mu\text{m}$. The resolving power R was around 350 at $2.2 \mu\text{m}$. The slit width we used is $0.''6$, slightly wider than the seeing size, so that the effective spectral resolution might change by seeing size. We measured FWHMs of the absorption features in each spectrum for each object, and confirmed that the FWHMs do not change in 1 pixel resolution ($\sim 6 \text{ \AA}$). Therefore, the effective spectral resolution was stable during observations of each target. The integration time used for each source was typically 60 – 300 seconds depending on source brightness. 8 or 12 exposures were taken for each object with the telescope dithered approximately $7.''5$ along the slit for sky subtraction. For the binary candidates, SAO 76542 was observed for correction of the effects of telluric absorption. For late-type dwarfs, we observed stars with spectral types of A0V – A3V at similar airmass. Exposures of an incandescent lamp on and off were taken at the end of each night as dome flats. Exposures of an argon lamp were taken for wavelength calibrations at the end of each night.

3. Data Reduction and Results

The Image Reduction and Analysis Facility (IRAF) software was used for all data reduction. Reduction procedure is similar for both UKIRT and Subaru data. First, a dithered pair of object frames were subtracted by each other, then divided by flat fields. Next, the data frames were geometrically transformed to correct the curvature of the slit image caused by the grating. The solutions of the geometric transformation and the wavelength calibration were derived from the spectrum of a krypton lamp or argon lamp taken closest in time to the object. Then, individual spectra were extracted from the transformed images using the APALL task. The region where the intensity of the object was more than 20 % of the peak intensity at each wavelength was summed into a one-dimensional spectrum. Extracted spectra were then normalized and combined to produce the final spectra. Low signal-to-noise spectra due to the tracking error of the telescope were rejected. The object spectrum was divided by the standard star spectrum, in which Brackett γ absorption line at $2.166 \mu\text{m}$ was removed by interpolating across the adjacent continuum with the SPLOT task. Finally the spectrum was multiplied by a blackbody spectrum of the temperature appropriate to the spectral type of the standard star (000 [cite]cite.TokunagaTokunaga(2000)).

The K -band spectra of the 23 YSO candidates, 5 companion candidates, 3 CTTSs, a protostar, and 10 late-type dwarfs are shown in figures 1 and 2. Prominent features in the spectra are the HI Br γ ($2.17 \mu\text{m}$), $2.21 \mu\text{m}$ feature, $2.26 \mu\text{m}$ feature, CO band ($2.29 \mu\text{m}$ and longer), and H_2O absorption ($<2.15 \mu\text{m}$ and $>2.3 \mu\text{m}$).

Equivalent widths of the Br γ line, the $2.21 \mu\text{m}$ feature, and the $2.26 \mu\text{m}$ feature were measured with SPLOT task by Gaussian fitting. On the other hand, equivalent widths

Table 1. The YSO sample in Heiles Cloud 2

ITG No.	$\alpha(1950)$	$\delta(1950)$	K	J-H	H-K	A_v	Obs.*	Identification [†]
2	4 ^h 34 ^m 57 ^s 0	25°53'01"	10.05±0.01	0.84±0.01	0.60±0.01	0.14±0.49	U	
4	4 35 15.0	26 01 28	11.05±0.02	2.07±0.05	1.29±0.03	11.42±0.55	U	
5	4 35 17.1	25 46 06	8.31±0.00	1.17±0.01	0.72±0.01	3.38±0.47	U	Kim 1-19
6	4 35 17.5	26 03 19	10.37±0.01	0.96±0.02	0.87±0.02	0.14±0.49	U	GM Tau
9A	4 35 56.6	25 27 17	12.53±0.03	0.88±0.04	0.66±0.04	0.27±0.42	S	
9B	4 35 56.6	25 27 21	14.45±0.03	0.70±0.04	0.70±0.04	0.00±0.39	S	separation = 4"31
13	4 36 15.2	25 31 44	11.69±0.02	0.84±0.03	0.55±0.03	0.36±0.51	U	
15A	4 36 40.5	25 56 02	9.02±0.00	0.86±0.01	0.62±0.01	0.19±0.47	U,S	
15B	4 36 40.4	25 56 06	14.50±0.01	1.01±0.02	0.73±0.02	1.48±0.39	S	separation = 2"99
17	4 36 43.1	25 55 49	10.37±0.01	0.96±0.02	0.82±0.02	0.45±0.49	U	
18	4 36 46.3	25 41 02	10.27±0.01	1.96±0.03	1.18±0.02	10.6±0.50	U	
21	4 36 57.5	25 50 38	10.83±0.01	1.49±0.03	0.94±0.02	6.21±0.51	U	GKH 5
24	4 37 03.6	26 01 26	13.05±0.05	1.01±0.09	0.70±0.09	1.65±0.82	U	
25A	4 37 03.8	25 59 38	8.97±0.00	1.97±0.01	1.37±0.01	9.82±0.49	U,S	IRAS 04370+2559
25B	4 37 03.6	25 59 36	13.38±0.01	2.14±0.01	1.28±0.01	12.29±0.38	S	separation = 4"29
27	4 37 32.7	25 52 34	8.46±0.00	1.04±0.00	0.64±0.00	2.28±0.47	U	
28	4 37 46.2	25 13 16	11.87±0.02	0.81±0.04	0.53±0.04	0.09±0.54	U	
29	4 37 52.5	25 16 19	10.74±0.01	0.86±0.01	0.54±0.01	0.63±0.49	U	
33A	4 38 04.2	25 50 23	11.50±0.02	1.41±0.04	1.19±0.03	3.94±0.55	U,S	
33B	4 38 04.1	25 50 28	16.05±0.02	0.79±0.04	0.54±0.03	0.00±0.41	S	separation = 5"17
36	4 38 10.0	25 12 27	11.01±0.02	0.86±0.02	0.54±0.02	0.63±0.49	U	
39	4 38 16.4	25 28 24	11.80±0.02	1.01±0.03	0.66±0.03	1.88±0.51	U	
40	4 38 20.8	25 38 10	11.47±0.02	2.80±0.18	1.99±0.05	16.68±0.83	U	GKH 32
41	4 38 34.6	25 50 46	9.72±0.01	1.66±0.01	1.11±0.01	7.38±0.49	U	IRAS 04385+2550
43	4 38 39.8	25 27 30	11.24±0.01	0.84±0.01	0.53±0.01	2.97±0.55	U	
45A	4 38 45.3	25 42 37	12.77±0.05	0.90±0.06	0.73±0.07	0.21±0.52	S	
45B	4 38 45.2	25 42 37	15.76±0.05	1.33±0.08	0.91±0.09	4.42±0.62	S	separation = 2"29
46	4 38 52.3	25 47 16	11.01±0.01	0.83±0.01	0.52±0.01	0.41±0.49	U	

* U: UKIRT, S: Subaru

† GKH: te]cite.GomezGomez et al.(1994) ([cite]cite.GomezGomez et al.(1994)), Kim: te]cite.KimKim(1990) ([cite]cite.KimKim(1990))

of the CO(2-0) band and the CO(4-2) band were calculated by simple integration of the absorption intensity. The uncertainties were estimated from the continuum fit, in which locating the continuum level was the main factor contributing to the equivalent width uncertainty. We also calculated reddening-independent indices of the H₂O band strength Q , following te]cite.WilkingWilking et al.(1999) ([cite]cite.WilkingWilking et al.(1999)). For Koornneef's extinction law (000 [cite]cite.KoornneefKoornneef(1983)), the Q index is written as

$$Q = \left(\frac{F_1}{F_2}\right) \left(\frac{F_3}{F_2}\right)^{1.24} \quad (1)$$

where F_1 , F_2 , and F_3 are flux densities between 2.07 μm – 2.13 μm , 2.267 μm – 2.285 μm , and 2.40 μm – 2.45 μm , respectively.

The measured equivalent widths of the features and the strengths of the bands are tabulated in table 2. The signal-to-noise ratio derived from deviations between each exposure is typically 60 (table 2). For the latest dwarfs taken both with UKIRT and Subaru, shapes of the spectra are similar for both observations and most of the measured

equivalent widths and band strengths are within observational uncertainties.

4. Discussion

4.1. Identification as YSOs using the Br γ feature

We identified 12 sources as YSOs, whose Br γ feature is in emission or in flat (featureless). We regard a featureless spectrum around the Br γ line with uncertainty less than 2 \AA in equivalent width as flat. The line emission is probably due to accretion of matter from the circumstellar disk onto the star (e.g. 000 [cite]cite.NajitaNajita et al.(1996)).

The other 11 objects with Br γ absorption are, on the other hand, likely early-type field-stars. Equivalent widths of the Br γ absorption feature are 4 \AA – 15 \AA , consistent with the spectral types of B, A, and early F (000 [cite]cite.AliAli et al.(1995)). Their locations on the color-color diagram are close to that of early-type field stars. Figure 3 shows the color-color diagram of the YSO candidates and field stars identified by ITG toward Heiles Cloud 2. The objects with the Br γ absorption tend to be located near the boundary between

Table 2. Equivalent widths of the features and strengths of the band of the YSO candidates, the CTTSs, and the M dwarfs.

Object	Br γ [Å]	2.21 μm [Å]	2.26 μm [Å]	CO(2-0) [Å]	CO(4-2) [Å]	Q	Obs.*	S/N
ITG 2	0.0±0.8	2.18±0.39	1.00±0.16	6.20	7.80	0.51±0.00	U	70
ITG 4	6.80±0.25	0.0±0.3	0.0±0.1	0.98±0.01	U	90
ITG 5	4.24±1.50	0.80±0.26	1.44±0.28	2.71	1.97	0.83±0.01	U	90
ITG 6	-2.25±0.62	0.98±0.23	0.53±0.22	2.30	3.79	0.81±0.01	U	90
ITG 9A	0.0±0.5	2.42±0.04	2.38±0.08	3.45	4.72	0.89±0.02	S	300
ITG 9B	0±3	0±3	0.0±0.2	2.71	2.35	0.88±0.09	S	60
ITG 13	14.08±0.70	0.0±0.3	0.0±0.4	0.94±0.01	U	60
ITG 15A&B	-0.79±0.79	3.29±1.00	4.12±1.24	6.73	10.39	0.64±0.01	U	80
ITG 15A	-3.93±1.08	3.29±0.24	3.19±0.30	5.88	9.79	0.61±0.00	S	460
ITG 15B	0.0±2.5	3.53±2.92	14.19±12.37	25.90	26.40	1.65 ^{+1.41} _{-0.82}	S	9
ITG 17	0.0±0.5	1.96±0.37	2.48±0.17	6.79	10.02	0.57±0.01	U	30
ITG 18	8.25±0.62	0.0±0.3	0.0±0.3	0.98±0.01	U	80
ITG 21	-3.8±3.8	2.22±0.78	2.31±0.44	5.11	8.50	0.54±0.01	U	70
ITG 24	6.60±1.69	0.0±0.5	0.58±0.12	1.03±0.01	U	40
ITG 25A&B	-5.34±0.91	1.94±0.51	2.54±0.50	3.72	5.43	0.87±0.03	U	100
ITG 25A	-12.63±0.22	3.38±0.16	2.26±0.08	3.52	8.26	0.89±0.02	S	290
ITG 25B	0.0±3.4	1.41±0.60	2.53±1.13	9.61	21.31	0.73±0.09	S	60
ITG 27	0.0±1.2	1.36±0.64	1.33±0.70	7.87	8.50	0.86±0.01	U	100
ITG 28	5.52±0.72	0.75±0.15	0.0±0.4	1.00±0.01	U	50
ITG 29	11.54±0.80	0.47±0.12	0.0±0.1	0.96±0.01	U	65
ITG 33A&B	-2.83±1.05	3.68±0.43	3.76±0.37	6.16	8.56	0.74±0.01	U	55
ITG 33A	-5.85±0.85	3.78±0.54	3.92±0.47	6.02	7.35	0.73±0.01	S	660
ITG 33B	0.0±2.9	7.54±4.90	...	0±9	...	0.90±0.04	S	20
ITG 36	5.14±1.63	1.20±0.43	1.26±0.33	0.91±0.01	U	50
ITG 39	7.40±0.70	0.0±0.2	0.0±0.2	1.00±0.02	U	60
ITG 40	0.0±0.9	4.15±1.00	1.78±0.53	4.95	10.76	0.67±0.02	U	30
ITG 41	0.0±1.0	2.31±0.50	2.08±0.56	3.43	6.53	0.93±0.01	U	100
ITG 43	7.68±0.98	0.0±0.4	0.0±0.2	0.97±0.01	U	60
ITG 45A	8.26±0.96	0.0±0.88	0.0±1.8	0.88±0.07	S	80
ITG 45B	0±25	0±4	0±9	1.55 ^{+1.77} _{-0.83}	S	6
ITG 46	0.0±1.0	1.46±0.50	1.34±0.33	11.13	13.69	0.80±0.01	U	70
DD Tau (M1)	-2.53±0.35	1.99±0.42	1.84±0.25	3.21	4.93	0.82±0.01	U	100
GH Tau (M2)	-0.58±0.57	2.91±0.46	2.81±0.48	5.01	6.92	0.85±0.01	U	130
FP Tau (M5.5)	-1.02±0.46	±0.013.35±0.69	3.47±0.38	6.91	8.27	0.75±0.00	U	150
IRAS 04365+2535	-1.68±0.94	0.0±0.2	0.0±0.2	1.06±0.02	U	160
GJ 380 (K5)	-0.14±0.25	4.20±0.19	4.14±0.25	6.28	9.56	0.93±0.01	S	630
GJ 96 (M1)	-1.80±1.80	4.78±1.18	4.24±0.24	6.67	7.19	0.84±0.01	U	110
GJ 205 (M1.5)	0.00±0.47	7.16±0.51	5.80±0.30	4.37	8.31	0.87±0.01	S	780
GJ 85.1 (M3)	-1.04±0.74	2.60±0.60	1.97±0.39	3.74	5.11	0.66±0.01	U	310
GJ 806 (M3)	-0.40±0.40	4.08±0.34	3.97±0.36	4.88	7.39	0.81±0.01	U	100
GJ 251 (M3)	0.0±0.1	5.67±0.47	4.01±0.20	4.90	8.08	0.77±0.01	S	620
GJ 12 (M5)	0.0±0.7	4.39±0.34	3.37±0.27	0.71±0.01	U	60
GJ 406 (M6)	-1.72±0.76	7.67±0.75	1.65±0.15	8.13	7.96	0.55±0.01	U	60
GJ 406 (M6)	0.0±0.1	7.23±0.31	2.10±0.95	6.02	7.35	0.60±0.00	S	510
LHS 2397a (M8)	0.0±0.7	4.98±0.31	0.39±0.07	14.32	13.54	0.51±0.01	U	90
LHS 2397a (M8)	-2.10±1.19	5.04±0.15	0.24±0.24	11.44	12.79	0.51±0.01	S	420
BRI 0021-214 (M9.5)	0.0±0.3	2.87±0.52	1.75±0.82	11.54	10.59	0.52±0.01	U	70
BRI 0021-214 (M9.5)	0.0±0.6	2.98±0.26	0.05±0.02	9.57	7.60	0.49±0.01	S	200

* U: UKIRT, S: Subaru

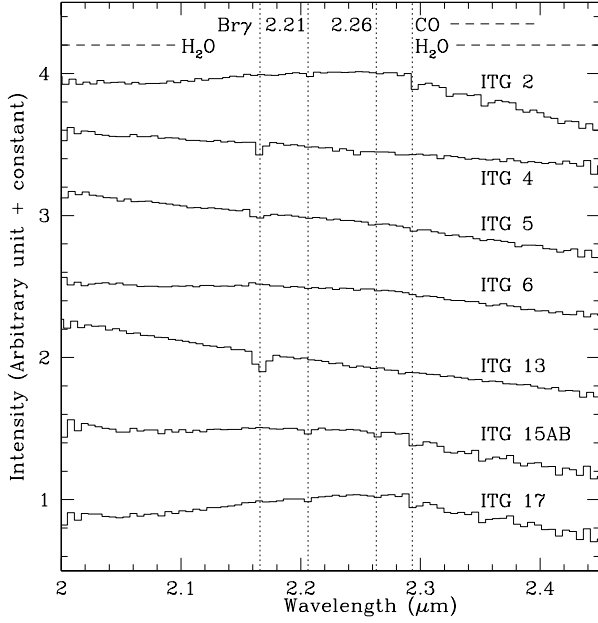


Fig. 1. (a) *K*-band spectra of the YSO candidates taken with UKIRT. The spectra are normalized by the flux between 2.18 μm and 2.20 μm , then offset in steps of 0.5.

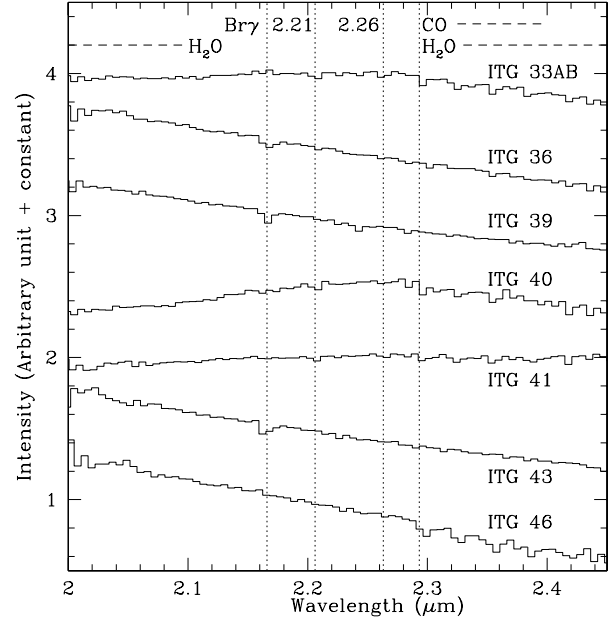


Fig. 1. (c) *K*-band spectra of the YSO candidates taken with UKIRT. The spectra are offset in steps of 0.5.

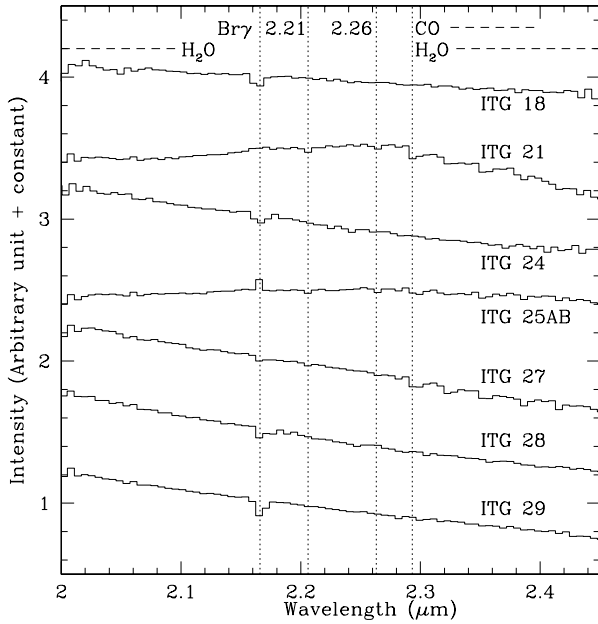


Fig. 1. (b) *K*-band spectra of the YSO candidates taken with UKIRT. The spectra are offset in steps of 0.5.

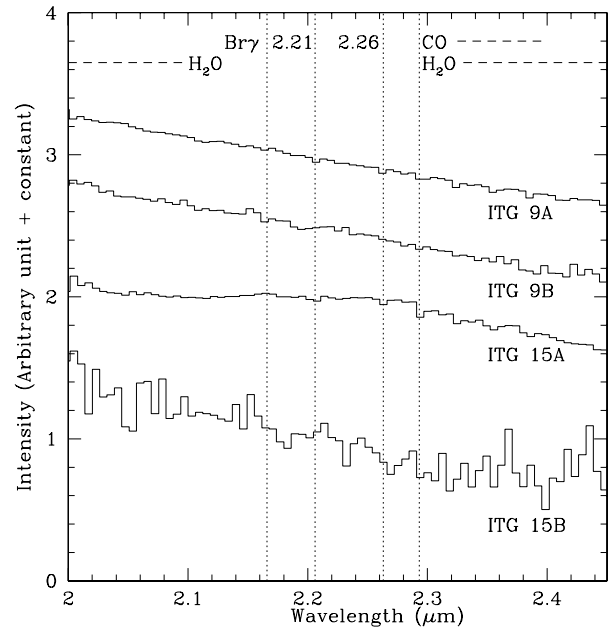


Fig. 1. (d) *K*-band spectra of the YSO binary candidates taken with Subaru. Additive constants for the spectra are 0, 1, 1.5, and 2, respectively.

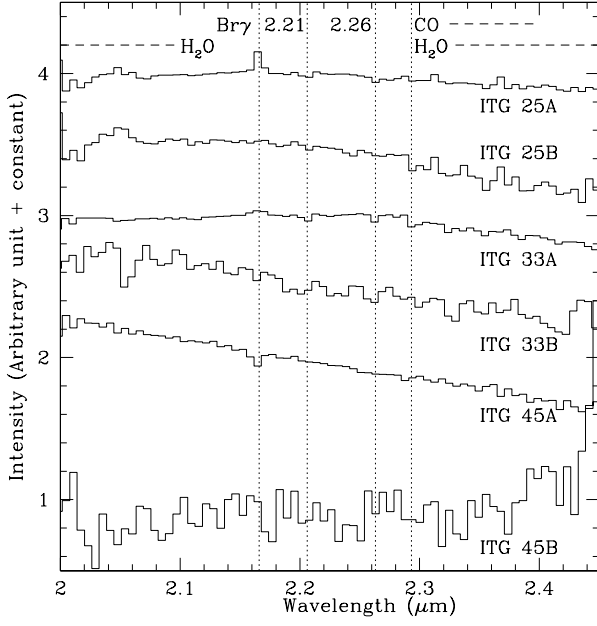


Fig. 1. (e) *K*-band spectra of the YSO binary candidates taken with Subaru. Additive constants are 0, 1, 1.5, 2, 2.5, and 3.

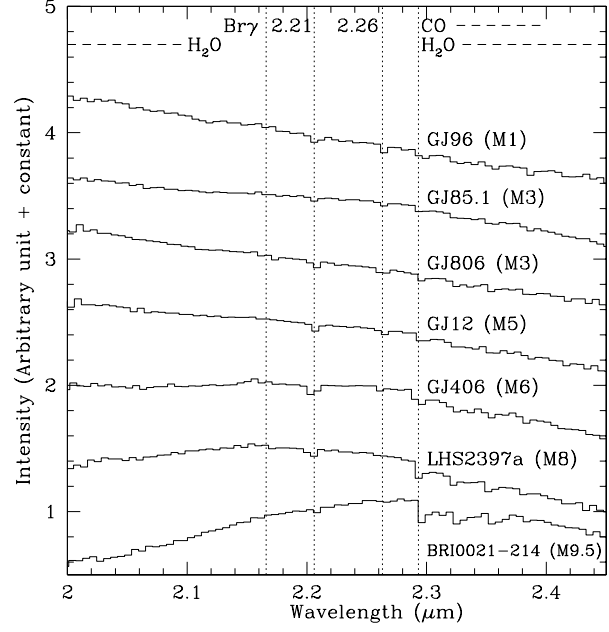


Fig. 2. (b) The *K*-band spectra of late-type dwarfs taken with UKIRT. The spectra are offset in steps of 0.5.

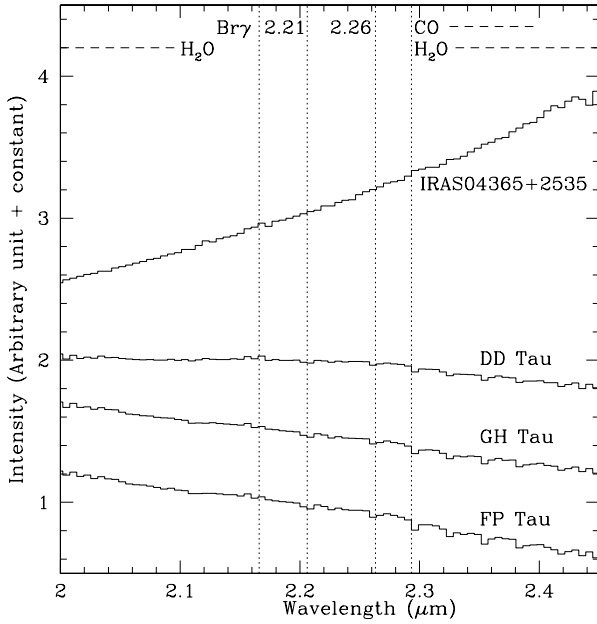


Fig. 2. (a) *K*-band spectra of CTTSs and a protostar taken with UKIRT. The spectra are normalized by the flux between 2.18 μm and 2.20 μm . Additive constants for the spectra are 0, 0.5, 1, and 2, respectively.

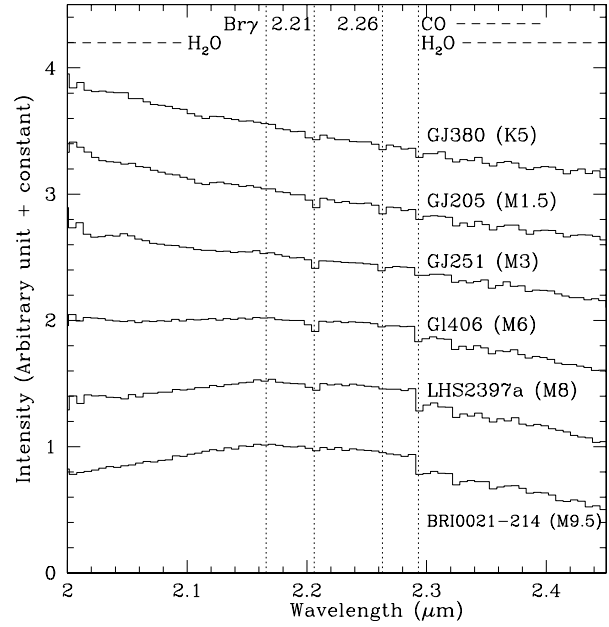


Fig. 2. (c) *K*-band spectra of late-type dwarfs taken with Subaru. The spectra are offset in steps of 0.5.

the "YSO region" and the "field-star region". Therefore, these objects may be early-type field-stars and have been misidentified as YSO candidates by photometric classification. The star count model of te[cite].Jones81Jones et al.(1981) ([cite]cite.Jones81Jones et al.(1981)) predicts 9 B- and A-type stars for $K < 12$ in a $1^\circ \times 1^\circ$ region toward Heiles Cloud 2. This predicted number is consistent with the observational number of the early type stars. Note that the number of such early-type stars does not increase for $K > 12$ toward high latitude direction such as the Taurus molecular cloud.

The uncertainty of the slope of the reddening vector may also account for the misidentification. For the Taurus molecular cloud, the smallest value of $E(J-H)/E(H-K)$ is 1.58 (000 [cite]cite.EliasElias(1978)), whereas the highest is 2.0 (000 [cite]cite.GomezGomez et al.(1994)). From photometric study alone, identification of YSOs depends on the extinction law especially for the objects near the boundary between the YSO region and the field star region on the color-color diagram.

4.2. Effective Temperature

We first describe the possible K -band features with which the effective temperatures of the M dwarfs and giants are derived. We then apply this method to the YSOs to derive their effective temperatures.

For cooler objects the conversion from MK spectral type to effective temperature is not straightforward because models do not exist to give the spectral type vs. effective temperature for pre-main sequence stars. Because the YSOs have luminosity class between dwarfs and giants, as we discuss below, we use the conversions both for dwarfs and for giants. In this paper we have adopted the conversions given by te[cite].TokunagaTokunaga(2000) ([cite]cite.TokunagaTokunaga(2000)) both for dwarfs and giants, te[cite].Bessell91Bessell(1991) ([cite]cite.Bessell91Bessell(1991)) for late M dwarfs, and te[cite].FluksFluks et al.(1994) ([cite]cite.FluksFluks et al.(1994)) for late M giants. As can be seen in figure 4, the difference in effective temperature is as much as 800K between M dwarfs and M giants even for the same spectral type.

4.2.1. 2.21 μm feature

The 2.21 μm feature consists mainly of Na, Sc, Si, and V absorption lines for late-type objects (000 [cite]cite.RamirezRamirez et al.(1997)). The low excitation energy of these lines makes it a strong absorption feature in M type stars. Figure 5 shows equivalent widths of the 2.21 μm feature of dwarfs and giants as a function of effective temperature. The equivalent widths increase with decreasing effective temperature. Moreover, dwarfs have larger equivalent widths than giants at the same effective temperature. The 2.21 μm feature has, therefore, a strong dependence on effective temperature and weak dependence on gravity (000 [cite]cite.KleinmannKleinmann & Hall(1986); 000 [cite]cite.TerndrupTerndrup et al.(1991); 000 [cite]cite.RamirezRamirez et al.(1997)).

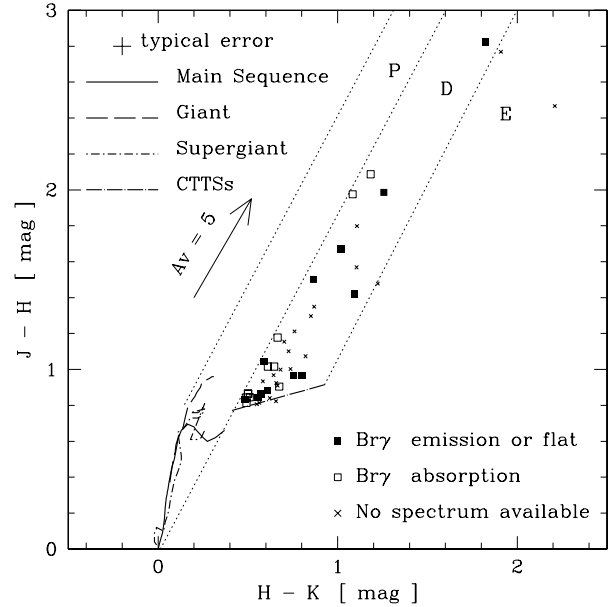


Fig. 3. The color-color diagram for Heiles Cloud 2. The intrinsic colors of main-sequence stars, giants (000 [cite]cite.Bessell88Bessell & Brett(1988)), supergiants (000 [cite]cite.TokunagaTokunaga(2000)), and CTTSs (000 [cite]cite.Meyer97Meyer et al.(1997)) are plotted with the reddening vector (000 [cite]cite.KoornneefKoornneef(1983); $E(J-H)/E(H-K)=1.7$ in the CIT system). All colors are transformed to the Johnson/Glass system (000 [cite]cite.Bessell88Bessell & Brett(1988)). Following the scheme discussed by te[cite].Strom93Strom et al.(1993) ([cite]cite.Strom93Strom et al.(1993)), the near-infrared sources are classified into three groups. In the "P" (photosphere) region on the color-color diagram, located are main sequence stars, giants, weak-line T Tauri (000 [cite]cite.TokunagaTokunaga(2000)) objects, and the CTTSs whose near-infrared excess is small. In the "D" (disk) region, a part of CTTSs are located. Protostars are located in the "E" (envelope) region on the color-color diagram. The objects located in the "D" region or the "E" region were identified as YSO candidates by the previous photometric study (ITG). The objects without absorption (i.e. with emission or in flat) in the $\text{Br}\gamma$ line are denoted by filled squares, as well as the objects with absorption by open squares. The YSO candidates without the spectroscopic observations are plotted by crosses. Field stars identified by ITG are shown by dots.

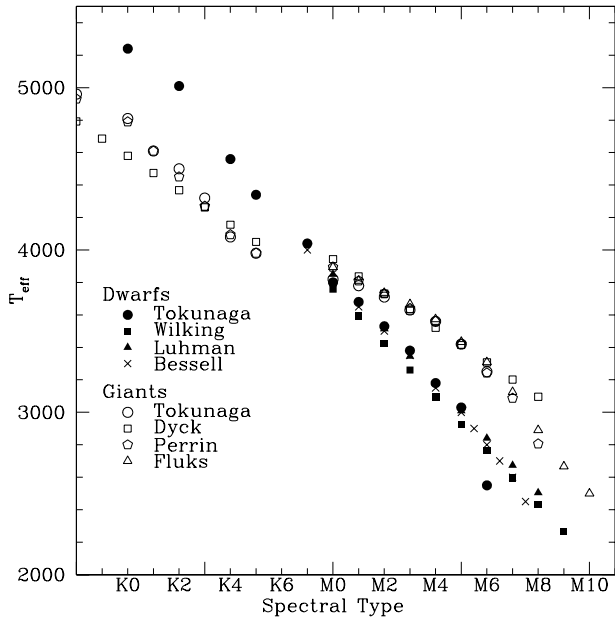


Fig. 4. Relation between effective temperature and spectral type for dwarfs and giants. Data are taken from Tokunaga & Tokunaga (2000) (Tokunaga & Tokunaga (2000)), Wilking & Wilking et al. (1999) (Wilking & Wilking et al. (1999)), Luhman & Rieke (1998) (Luhman & Rieke (1998)), Bessell (1991) (Bessell (1991)), Dyck & Dyck et al. (1998) (Dyck & Dyck et al. (1998)), Perrin & Perrin et al. (1998) (Perrin & Perrin et al. (1998)), and Fluks & Fluks et al. (1994) (Fluks & Fluks et al. (1994)).

Near-infrared Na lines of CTTSs have symmetric profile, indicating photospheric origin (Greene & Lada (1997)), while optical Na lines are red-shifted, indicating outflow origin (Gullbring & Gullbring et al. (1996)).

4.2.2. 2.26 μm feature

The 2.26 μm feature consists mainly of Ca, Si, and Ti lines for late-type objects (Ramirez & Ramirez et al. (1997)). Figure 6 shows equivalent widths of the 2.26 μm feature of dwarfs and giants as a function of effective temperature. The 2.26 μm feature has a peak in its equivalent width around 3500 K, then its width decreases with decreasing temperature, due to moderate excitation energy of Ca. This feature has also strong dependence on effective temperature, and weak dependence on gravity (Ramirez & Ramirez et al. (1997)).

4.2.3. Ratio of Metallic features

Use of ratio of feature strengths to derive effective temperature can avoid not only the effect of metallicity but also the effect of veiling if features whose wavelengths are close with each other are selected (Meyer (1996)). We have checked if the 2.21 μm feature and the 2.26 μm feature can be used as

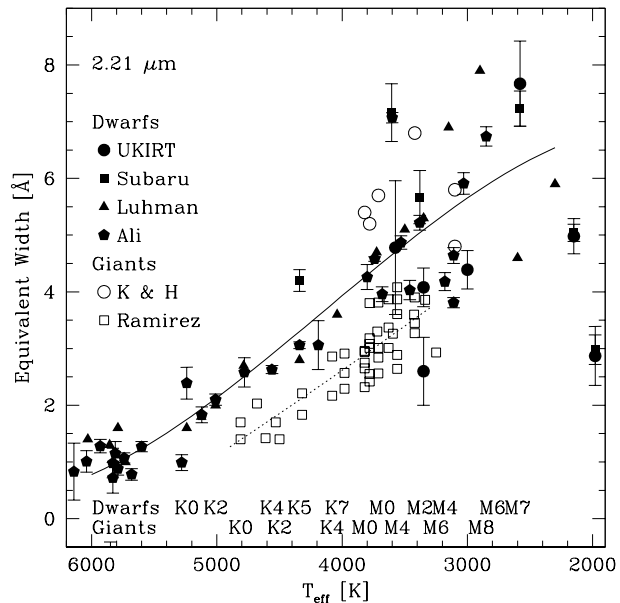


Fig. 5. Equivalent widths of the 2.21 μm feature as a function of effective temperature. Data are taken from Luhman & Rieke (1998) (Luhman & Rieke (1998)), Ali et al. (1995) (Ali et al. (1995)), Kleinmann & Hall (1986) (Kleinmann & Hall (1986)), Ramirez & Ramirez et al. (1997) (Ramirez & Ramirez et al. (1997)), and this paper. Filled symbols represent the equivalent widths for dwarfs and open symbols for giants. A solid line shows a fitted line for dwarfs with $T_{\text{eff}} > 2300$ K, and a dotted line for giants listed in Ramirez & Ramirez et al. (1997) (Ramirez & Ramirez et al. (1997)).

a ratio index of effective temperature. Figure 7 shows the 2.26 μm / 2.21 μm feature ratio for dwarfs and giants as a function of effective temperature. Although the scattering is relatively large and no data is available for cool giants, the ratio decreases as the temperature decreases. Dwarfs and giants have similar values, so that surface gravity does not appear to significantly affect this feature ratio. Therefore, this feature ratio is a sensitive indicator of effective temperature for $T_{\text{eff}} < 3300$ K. For 2.26 μm / 2.21 $\mu\text{m} > 1$, only lower limits of effective temperature can be estimated.

4.2.4. H₂O

The H₂O absorption bands in the near-infrared wavelengths are a sensitive function of effective temperature for cool stars (Aaronson & Aaronson et al. (1978); Jones & Jones et al. (1994)). Figure 8 shows the water index Q of the dwarfs taken from our observations, as well as those of dwarfs and giants taken from Lançon & Rocca-Volmerange (1992) (Lançon & Rocca-Volmerange (1992)). A dotted line represents a fitted line of the Q index for the dwarfs and

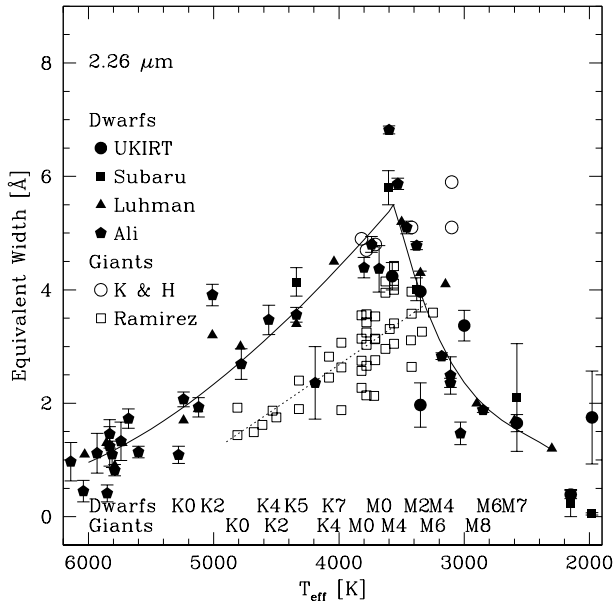


Fig. 6. Equivalent width of the $2.26 \mu\text{m}$ feature as a function of effective temperature. Filled symbols represent the equivalent widths for dwarfs and open symbols for giants. Solid lines show fitted lines for dwarfs, and a dotted line for giants listed in Ramirez et al. (1997). The intensity has a peak at 3500 K for dwarfs.

a dashed line for the giants. In this figure, the relation between the Q index and spectral type for M dwarfs derived by Wilking et al. (1999) also shown by a solid line. While Wilking's relation is consistent with the plotted Q index for the dwarfs, the Q indices for giants are much smaller than the Wilking's relation. Since the YSOs have surface gravity between dwarfs and giants, as we discuss below, we should use both the relation for the dwarfs and that for the giants to estimate effective temperature of the YSOs. Note that the veiling effect by a circumstellar disk could increase the Q index, leading to higher temperatures.

4.2.5. Effective Temperatures of the YSOs

The effective temperatures of the observed YSOs and their companions are derived using the $2.26 \mu\text{m} / 2.21 \mu\text{m}$ feature ratio and the Q index ($T_{\text{eff}}(\text{NIR})$ in table 3). The effective temperatures of most YSOs are less than 4000 K, lower than that of typical CTTSs.

The effective temperatures of the observed CTTSs are also derived from the near-infrared features. The effective temperatures estimated from the near-infrared spectroscopy are consistent with those converted from optical spectral types for all the CTTSs.

4.3. Luminosity Class

Since the $2.21 \mu\text{m}$ feature and the $2.26 \mu\text{m}$ feature are primarily sensitive to effective temperature, and

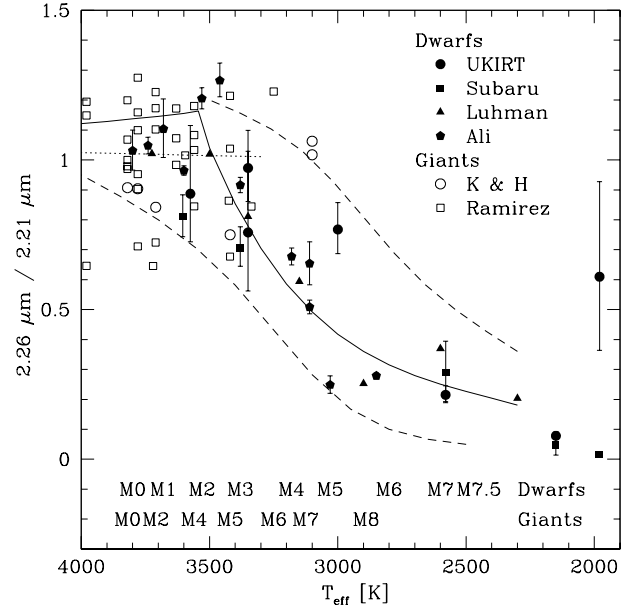


Fig. 7. Ratio of the $2.26 \mu\text{m}$ feature to the $2.21 \mu\text{m}$ feature as a function of effective temperature. Data are taken from our UKIRT observations, Subaru observations, Luhman & Rieke (1998), Luhman & Rieke (1998), Ali et al. (1995), Kleinmann & Hall (1986), and Ramirez et al. (1997). Solid lines show the ratio for dwarfs, and a dotted line for giants, both derived from the fitted lines in figures 5 and 6. Dashed lines show the conversions used for estimate of the upper limit and the lower limit of effective temperature of the YSOs.

the depth of the CO band varies with surface gravity, the luminosity class of the object is estimated from a plot of the equivalent widths of these atomic features against the widths of the CO band. Figure 9 shows the sum of the equivalent widths of the $2.21 \mu\text{m}$ feature and the $2.26 \mu\text{m}$ feature against the CO band equivalent width of the YSOs, the CTTSs, and the late-type dwarfs. A sum of the equivalent widths of the CO (2-0) and CO (4-2) bands is used as a CO equivalent width. CO (3-1) band is not included because it contains a sodium line (Kleinmann & Hall (1986)). Relationships for giants and dwarfs (Greene & Meyer (1995)) are also shown in the figure by the solid lines. Their fits are only applied to stars with spectral types $< M6V$ and $< M2III$, and cannot be applied to very late-type stars. Points of very late-type dwarfs are close to the line for giants, since their equivalent width of the $2.26 \mu\text{m}$ feature diminishes (see figure 6).

Most of the YSOs lie, like the CTTSs, between these two lines. Therefore most of the YSOs and the CTTSs have a luminosity class between dwarfs and giants, classified as luminosity class IV.

Table 3. Effective temperatures and spectral types of the YSOs and the CTTSs.

Object	$T_{\text{eff}}(\text{ratio})^*$ [K]	$T_{\text{eff}}(2.21)^\dagger$ [K]	$T_{\text{eff}}(2.26)^\ddagger$ [K]	$T_{\text{eff}}(Q)^\S$ [K]	$T_{\text{eff}}(\text{NIR})^\parallel$ [K]	$T_{\text{eff}}(\text{Opt})^\#$ [K]	Sp.(V)**	Sp.(III) ^{††}	$\log L_{\text{bol}}^{\ddagger\ddagger}$ [L_\odot]
ITG 2	2300~3400	<5200	...	2400~3200	2400~3200		M4~M8	>M6	-1.11 ~ -0.81
ITG 4	field-star								
ITG 5	field-star								
ITG 6	2300~3700	3500~3700	3500~3700		M1~M2	M2~M4	-1.72 ~ -1.42
ITG 9A	>3000	>3700	>3700		<M1	<M1	
ITG 9B	>3600	>3600		<M2	<M4	
ITG 13	field-star								
ITG 15A&B	>3000	<4800	<4700	3000~3600	3000~3600		M2~M5	M4~M7.5	-0.95 ~ -0.65
ITG 15A	>3000	2900~3500	3000~3500		M2~M5	M5~M7.5	-0.95 ~ -0.65
ITG 15B	>3100	
ITG 17	2700~3400	2700~3400		M3~M6.5	>M5	-1.49 ~ -1.19
ITG 18	field-star								
ITG 21	>2900	2600~3200	2900~3200		M4~M5	M6~M7.5	-1.36 ~ -1.06
ITG 24	field-star								
ITG 25A&B	>3250	3600~4800	3600~4800		K3~M1	K0~M2	-0.69 ~ -0.39
ITG 25A	2700~3600	>3700	2700~3600		M2~M6.5	M4~M8	-0.57 ~ -0.27
ITG 25B	2900~4400	2900~4400		K5~M5	K3~M8	-2.23 ~ -1.93
ITG 27	>2500	3600~4800	3600~4800		K3~M1	K0~M2	-0.44 ~ -0.14
ITG 28	field-star								
ITG 29	field-star								
ITG 33A&B	>3200	<4400	<4400	3300~4100	3300~4100		K7~M3	K4~M6	-2.02 ~ -1.72
ITG 33A	3200~4000	3200~4000		M0~M4	M0~M6	-2.02 ~ -1.72
ITG 33B	>3700	>3700		<M1	<M0	
ITG 36	field-star								
ITG 39	field-star								
ITG 40	2000~3400	<4400	...	3000~3700	3000~3400		M3~M5	M5~M7.5	-1.50 ~ -1.20
ITG 41	>2750	>3800	>3800		<M0	<M0	
ITG 43	field-star								
ITG 45A	field-star								
ITG 45B	>3200	>3200		<M4	<M6	
ITG 46	>2700	3500~4500	3500~4500		K4~M2	K2~M4	-1.63 ~ -1.33
DD Tau	>2900	3500~4500	3500~4500	3700~3900	K4~M2	K2~M4	
GH Tau	>2900	<4800	...	3600~4800	3600~4800	3500~3700	K3~M2	K0~M4	
FP Tau	>3100	<4700	<5000	3300~4100	3300~4100	2900~3700	K7~M3	K4~M6	

* T_{eff} estimated from the 2.26 μm / 2.21 μm feature ratio.

† T_{eff} estimated from the the equivalent widths of the 2.21 μm feature. Because YSOs are subject to continuum emission and the strength of the line increases with lower temperature, only the upper limit of the effective temperature can be estimated.

‡ T_{eff} estimated from the equivalent widths of the 2.26 μm feature.

§ T_{eff} estimated from the Q index. The range of temperatures for $T_{\text{eff}}(Q)$ includes estimates for both dwarf and giant surface gravities. These effective temperatures may be upper limits, due to veiling effect.

|| T_{eff} estimated from the 2.26 μm / 2.21 μm feature ratio and the Q index.

T_{eff} converted from optical spectral type.

** Estimated spectral type in the dwarf scale.

†† Estimated spectral type in the giant scale.

‡‡ Bolometric luminosity for the midpoint of $T_{\text{eff}}(\text{NIR})$, estimated from the previous photometric study (see §4.4.1).

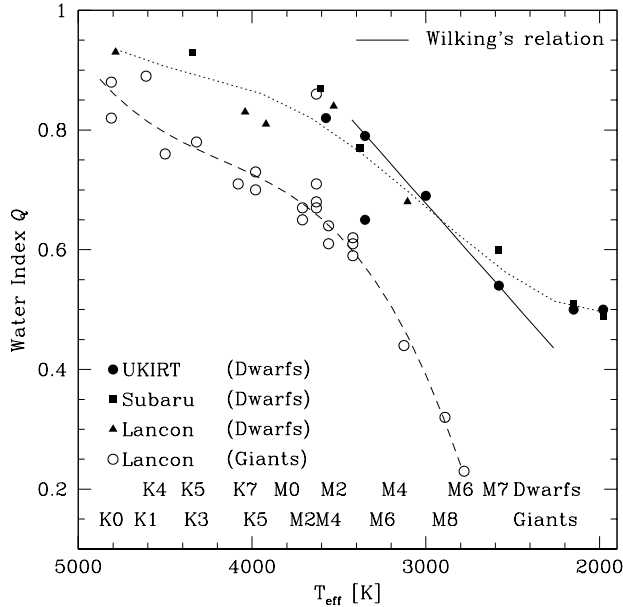


Fig. 8. The Q index as a function of effective temperature. Data are taken from our observations and from [Lançon & Rocca-Volmerange\(1992\)](#) ([Lançon & Rocca-Volmerange\(1992\)](#)). A solid line shows the relationship between the Q indices and spectral type for dwarfs ([Wilking et al.\(1999\)](#)). A dotted line shows a fitted line of the Q index for the dwarfs, and a dashed line for the giants.

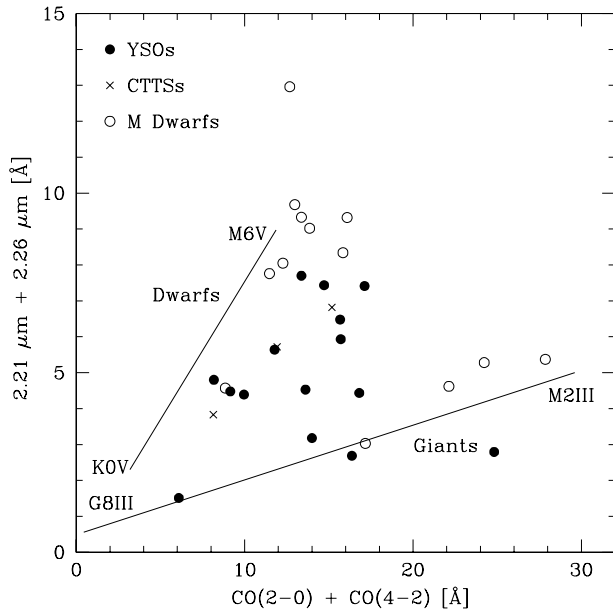


Fig. 9. Luminosity class of the YSOs. The combined equivalent width of the $2.21 \mu\text{m}$ feature and the $2.26 \mu\text{m}$ feature is plotted against the combined CO band equivalent width. Loci of dwarfs and giants ([Greene & Meyer\(1995\)](#)) are shown by solid lines.

4.4. Mass and Age of the YSOs

Based on the effective temperature described above and the bolometric luminosity described below, the masses of the YSOs and their companions are estimated with recent evolutionary tracks on the HR diagram.

4.4.1. Bolometric Luminosity

Bolometric luminosity of the YSOs is estimated from the J -band luminosity, because the J -band emission arises primarily from the photosphere of YSOs ([Bertout et al.\(1988\)](#)). First, the J -band luminosity of the YSOs is corrected for interstellar extinction on the color-color diagram (ITG). Next, three cases are assumed, where the fraction of the photospheric luminosity to the total luminosity is 1.0, 0.8, and 0.5 in the J -band. Then, by comparing the photospheric luminosity of the YSOs with that of late-type dwarfs in the J -band ([Leggett et al.\(1996\)](#)), the bolometric luminosity of the YSO's photosphere is estimated

This procedure has the following uncertainties.

1. Extinction of each YSO is corrected on the color-color diagram. If the extinction law of [Bessell & Brett\(1988\)](#) ([Bessell & Brett\(1988\)](#)) is used instead of [Koornneef\(1983\)](#) ([Koornneef](#)), a 6 % larger value is derived as visual extinction, making the intrinsic luminosity brighter by about 2 %.
2. Extinction is deduced from the distance between the observed color of the object and the intrinsic color of CTTSs on the color-color diagram. The intrinsic color of CTTSs deduced by [Meyer et al.\(1997\)](#) ([Meyer et al.\(1997\)](#)) has a dispersion as much as 0.17 mag in $J-H$, corresponding to an uncertainty of 1.5 mag in visual extinction or 0.16 dex in bolometric luminosity.
3. The intrinsic color of YSOs might be different from the intrinsic color of CTTSs. Central objects of the YSOs are M type stars whereas those of CTTSs are mainly K type stars. Color of an M type dwarf is about 0.1 mag redder than that of a K type dwarf both in $J-H$ and $H-K$.
4. We assumed that the distance to the Taurus molecular cloud is 140 pc. Hipparcos observations estimate 142 pc with an uncertainty of ± 14 pc as the distance to the cloud ([Wichmann et al.\(1998\)](#)). Therefore the uncertainty due to distance is ± 0.1 dex in bolometric luminosity.
5. The fractions of the photospheric luminosity are assumed to be 1.0, 0.8, and 0.5 of the total luminosity in the J -band. In these three cases, uncertainty is 0.3 dex in bolometric luminosity. If the fraction is smaller, photospheric luminosity is fainter. Although the fraction value could be deduced from veiling effect index r_J ([Greene & Meyer\(1995\)](#)), r_J has a large uncertainty for all YSOs due to rather large

observational uncertainties in the equivalent widths of the metallic features. Therefore, we did not employ r_J to estimate the photospheric luminosity.

4.4.2. HR diagrams

Several groups have recently developed and refined evolutionary tracks for low-mass stars, brown dwarfs, and even giant planets. Figures 10, 11, and 12 show the HR diagrams of the YSOs and their companions. Overlaid are the evolutionary tracks of [te\]cite.DM94D'Antona & Mazzitelli\(1994\)](#) ([\[cite\]cite.DM94D'Antona & Mazzitelli\(1994\)](#)), [te\]cite.DM98D'Antona & Mazzitelli\(1998\)](#) ([\[cite\]cite.DM98D'Antona & Mazzitelli\(1998\)](#)), and [te\]cite.BaraffeBaraffe et al.\(1998\)](#) ([\[cite\]cite.BaraffeBaraffe et al.\(1998\)](#)).

Mass and age for individual YSOs are estimated from the HR diagrams with the evolutionary tracks (table 4). Some YSOs are indeed very low-mass YSOs (typically $0.1 M_{\odot}$ – $0.3 M_{\odot}$). *These objects are definitively a different population from CTTSs in term of their mass.* The uncertainties in the mass are about a factor of 2 and those in the age are about a factor of 5 for the YSOs as shown in the figures. On the other hand, none of the mass and age of the companions are determined mainly due to the poor signal-to-noise ratio on the spectra. Additional notes are described in the appendix for most companions.

Mass-luminosity relation of the YSOs is shown in figure 13, where also shown are the mass-luminosity relations of CTTSs (000 [\[cite\]cite.Strom88Strom et al.\(1988\)](#)) and the predicted relations for three ages calculated from [te\]cite.BaraffeBaraffe et al.\(1998\)](#) ([\[cite\]cite.BaraffeBaraffe et al.\(1998\)](#)). Most of the YSOs are distributed within one order of magnitude in the ages. Both CTTSs and the YSOs have near-infrared excesses, implying existence of circumstellar disks. The ages of these objects indicate the survival time of the circumstellar disk, and it is interesting to ask whether the mass of the central object affects the evolution of circumstellar disk. The ages of most YSOs are less than 10^7 yr, similar to the age of CTTSs. However, since the mass-age relation of YSOs depends strongly on evolutionary tracks (figures 10, 11, 12, and table 4), we cannot conclude that disk survival time is independent on the mass of the central object.

The small amount of objects prevents us from making a mass function of the YSOs. In the four other regions but except for Heiles Cloud 2, [te\]cite.Luhman00Luhman\(2000\)](#) ([\[cite\]cite.Luhman00Luhman\(2000\)](#)) shows that the mass function has a peak at $0.8 M_{\odot}$ and is relatively flat between $0.1 M_{\odot}$ and $0.8 M_{\odot}$. [te\]cite.Briceno98Briceno \(1998\)](#) ([\[cite\]cite.Briceno98Briceno \(1998\)](#)), as well as [te\]cite.Luhman00Luhman\(2000\)](#) ([\[cite\]cite.Luhman00Luhman\(2000\)](#)) suggest a deficit of brown dwarfs in the regions, although [te\]cite.Martin01Martin et al.\(2001\)](#) ([\[cite\]cite.Martin01Martin et al.\(2001\)](#)) have identified four brown dwarfs in two sparsely populated stellar groups. Given a limiting magnitude of the ITG survey ($K = 13.4$) and an age of 1 Myr, we expect to

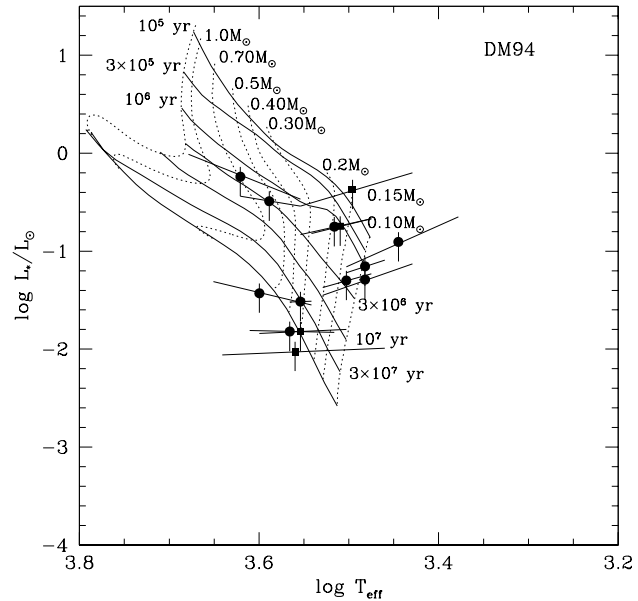


Fig. 10. The HR diagram of YSOs with the evolutionary tracks of [te\]cite.DM94D'Antona & Mazzitelli\(1994\)](#) ([\[cite\]cite.DM94D'Antona & Mazzitelli\(1994\)](#)) with the Alexander opacities and the CM convection overlaid. Filled circles and filled squares show the loci of the YSOs deduced from the UKIRT observations and from the Subaru observations, respectively. $T_{\text{eff}}(\text{NIR})$ in table 3 are adopted. Error bars are tilted, because the bolometric luminosity is a function of the J -band luminosity and the effective temperature (see §4.4.1).

reach a mass limit of $0.03 M_{\odot}$ for $A_v = 0$ with the survey. In order to take a census of brown dwarfs in Heiles cloud 2 and to construct an initial mass function of the cloud, a deeper spectroscopic search is required.

4.5. Comparison with other studies

[te\]cite.WilkingWilking et al.\(1999\)](#) ([\[cite\]cite.WilkingWilking et al.\(1999\)](#)) carried out K -band spectroscopic observations of low-luminosity sources in the ρ Oph cloud. They estimated spectral types of the objects using the Q index, then derived effective temperatures using the conversion for dwarfs. The effective temperature derived from their method is the same value as the lower limit of effective temperatures derived from the Q index in this paper. This is because M dwarfs have a higher temperature than M dwarfs even with the same Q index, due to gravity dependence of the water band depth (see figure 8). For example, ITG 40 has a Q of 0.67, which corresponds to a spectral type of M4.7 for Wilking's relation. This spectral type corresponds to 20300K in the dwarf scale, which is consistent with the lower limit on the effective temperature derived from the Q index in this paper.

They estimated extinction of each object from the $J-H$ color, assuming no infrared excesses in the J - and H -bands. This procedure could lead to a slightly higher value for extinction than our method. For example A_v of ITG 40

Table 4. Mass and age of the YSOs.

Object	DM94*		DM98†		BCAH98‡	
	mass [M_{\odot}]	age [10^6 yr]	mass [M_{\odot}]	age [10^6 yr]	mass [M_{\odot}]	age [10^6 yr]
ITG 2	<0.15	<2	0.05 – 0.18	<3	<0.2	<3
ITG 6	0.25 – 0.4	20 – 50§	0.35 – 0.45	>30§	0.4 – 0.5	>50§
ITG 15A&B	0.1 – 0.4	0.1 – 3	0.12 – 0.4	0.2 – 5	<0.55	<8
ITG 15A	0.1 – 0.3	0.1 – 3	0.12 – 0.3	0.2 – 4	<0.45	<5
ITG 17	<0.2	<10	0.08 – 0.3	0.3 – 20	<0.3	<20
ITG 21	<0.15	<2	0.11 – 0.19	1 – 5	<0.2	<4
ITG 25A&B	0.35 – 0.8	1 – 10	0.35 – 0.75	2 – 8	0.57 – 1.00	4 – 18
ITG 25A	<0.35	<1	0.09 – 0.35	<2	<0.57	<4
ITG 25B	>0.08	>10	>0.06	>4.5
ITG 27	0.3 – 1.2	1 – 5	>0.3	1 – 8	0.57 – 1.2	3 – 18
ITG 33A&B	>0.15	>10§	>0.2	>30§	>0.2	>30§
ITG 33A	>0.15	>10§	>0.2	>30§	>0.14	>18§
ITG 40	<0.2	1 – 7	0.14 – 0.3	2 – 15	0.1 – 0.32	4 – 18
ITG 41
ITG 46	>0.25	>20§	>0.35	>30§	>0.35	>30§

* [cite]DM94D'Antona & Mazzitelli(1994) ([cite]DM94D'Antona & Mazzitelli(1994)) with the Alexander opacities and the convection

† [cite]DM98D'Antona & Mazzitelli(1998) ([cite]DM98D'Antona & Mazzitelli(1998))

‡ [cite]BaraffeBaraffe et al.(1998) ([cite]BaraffeBaraffe et al.(1998))

§ These ages are discussed further in the appendix.

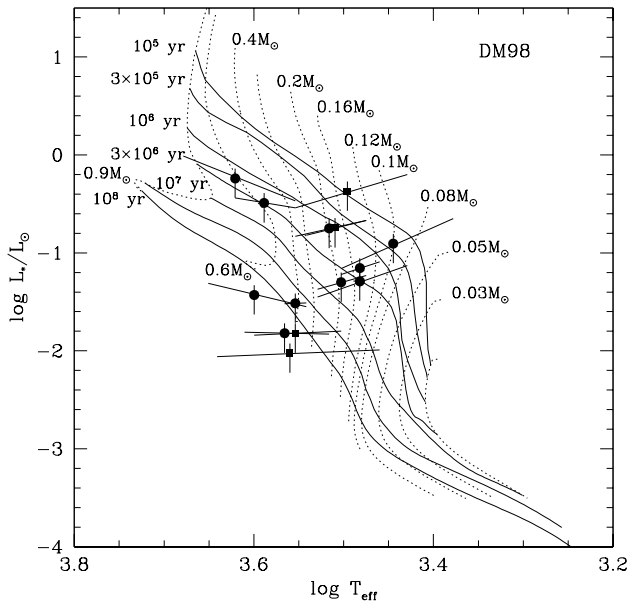


Fig. 11. The HR diagram of YSOs with evolutionary tracks of [cite]DM98D'Antona & Mazzitelli(1998) ([cite]DM98D'Antona & Mazzitelli(1998)) overlaid.

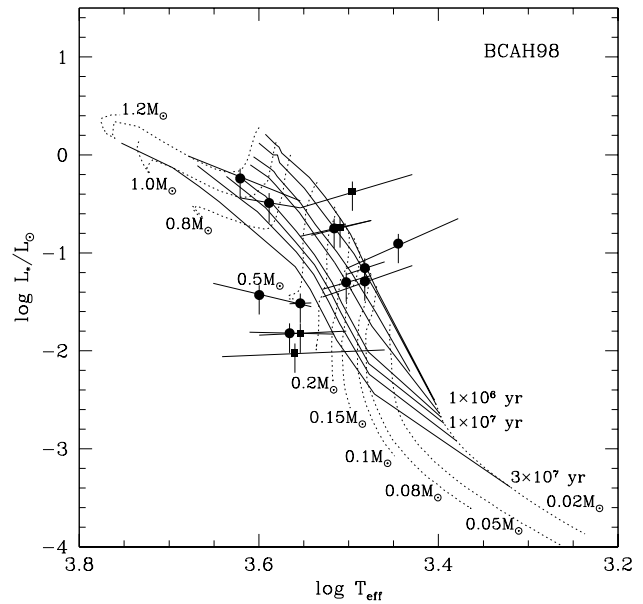


Fig. 12. The HR diagram of YSOs with evolutionary tracks of [cite]BaraffeBaraffe et al.(1998) ([cite]BaraffeBaraffe et al.(1998)) overlaid.

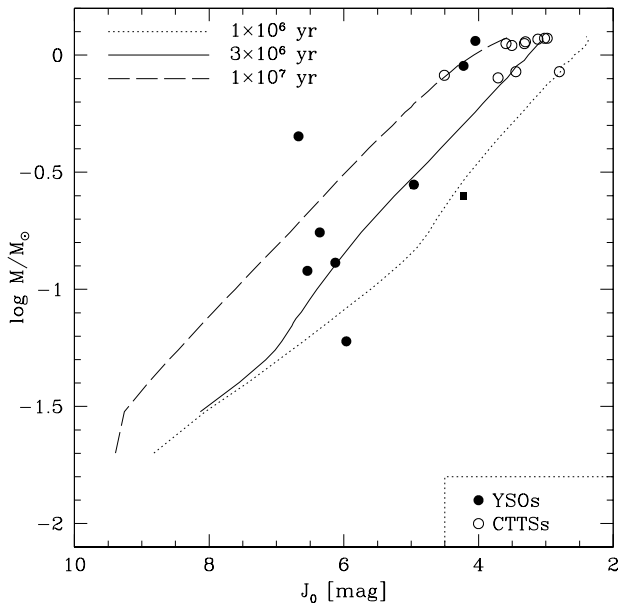


Fig. 13. Mass – absolute J -band magnitude relation of the YSOs and the CTTs listed in te]cite.Strom88Strom et al.(1988) ([cite]cite.Strom88Strom et al.(1988)). The J -band magnitudes were corrected for interstellar extinction on the color-color diagram (ITG). The mass of the YSOs and the CTTs are estimated from the evolutionary track of te]cite.BaraffeBaraffe et al.(1998) ([cite]cite.BaraffeBaraffe et al.(1998)). The distance modulus of the Taurus molecular cloud is 5.73 (000 [cite]cite.EliasElias(1978)).

is estimated to be 20.0 mag by their method. On the other hand, our value is 16.7 mag. Larger A_V leads to higher values in bolometric luminosity. Bolometric luminosity of ITG 40 is estimated to be $0.1 L_\odot$ by their method, whereas $0.05 L_\odot$ by us, even though discrepancy is within uncertainty.

te]cite.LuhmanRiekeLuhman & Rieke(1998) ([cite]cite.LuhmanRiekeLuhman & Rieke(1998)) carried out K -band spectroscopy of low-luminosity sources in the L 1495 cloud in Taurus. They derived the spectral type of the object by fitting the $2.21 \mu\text{m}$ feature and $2.26 \mu\text{m}$ strengths of the object to those of dwarf stars varying in amounts of veiling. With their method, spectral type of ITG 40 is estimated to be M3 or M7. Derived spectral type corresponds to $2600 \text{ K} \sim 3400 \text{ K}$, in agreement with our result.

5. Conclusions

1. We have carried out near-infrared spectroscopic observations of 23 very low-luminosity YSO candidates and 5 of their companions in Heiles Cloud 2 in the Taurus molecular cloud. Near-infrared spectroscopy is essential to characterize objects in the color-color diagram. Out of the 28 objects, 5 objects have $\text{Br}\gamma$ in emission and 7 have "flat" spectra over the $\text{Br}\gamma$ feature. We conclude that these 12 objects are in-

deed YSOs.

2. Compiling near-infrared spectra of dwarfs and giants taken by us as well as those in the literature, the ratio of the $2.26 \mu\text{m}$ feature to the $2.21 \mu\text{m}$ feature turns out to be a good indicator of the effective temperature for M type stars.
3. The effective temperatures of the YSOs are determined. These objects are cool ($T_{\text{eff}} < 4000 \text{ K}$) YSOs.
4. The mass of these YSOs is estimated from the HR diagram with recent evolutionary tracks. Some objects are very low-mass ($0.1 M_\odot - 0.3 M_\odot$) YSOs.
5. The age of these YSOs appears to be $10^5 - 10^7$ years. However, the deduced age depends on evolutionary track models.

We are grateful to T. Geballe, T. Kerr, and Y. Oasa for help with the UKIRT observations, and H. Terada, N. Kobayashi, and B. Potter for the Subaru observations. We thank T. Tsuji, and T. Nakajima for discussions on spectral features of late type stars. We also thank our referee, B. Wilking, for many helpful comments. Y. I. is supported from the Sumitomo Foundation. A part of this study was supported by the UK-Japan collaboration fund from the JSPS. The United Kingdom Infrared Telescope is operated by the Joint Astronomy Centre on behalf of the U.K. Particle Physics and Astronomy Research Council. Subaru Telescope is operated by the National Astronomical Observatory of Japan.

Appendix. Individual Objects

ITG 2

Mass of this object is estimated to be less than $0.2 M_\odot$ by any evolutionary track, possibly a young brown dwarf. Age of this object is estimated to be less than 3×10^6 .

ITG 6 (GM Tau)

te]cite.GomezGomez et al.(1994) ([cite]cite.GomezGomez et al.(1994)) derived the magnitude of this star as 8.06 in the K -band, one order of magnitude brighter than the magnitude derived by ITG and by te]cite.KenyonKenyon & Hartmann(1995) ([cite]cite.KenyonKenyon & Hartmann(1995)). If the bolometric luminosity is one order of magnitude brighter, the age of this star is estimated to be around 10^6 yr, while the mass of the star is still about $0.3 M_\odot$.

te]cite.KenyonKenyon & Hartmann(1995) ([cite]cite.KenyonKenyon & Hartmann(1995)) classified spectral type of this star as "continuum". Therefore the spectrum of this object has a large amount of veiling. Since only the lower limit of the effective temperature is estimated from the Q

index, true effective temperature might be lower than that estimated here. If half of the K -band flux comes from a circumstellar disk, for example, the Q index changes from 0.81 to 0.62 and the effective temperature to 2700 K \sim 3500 K. This value is not inconsistent with the effective temperature deduced from the ratio of the 2.26 μm feature to the 2.21 μm feature. With this temperature, the mass and the age of the object would be 0.1 M_{\odot} and 3×10^6 yr.

ITG 9

The fact that both spectra of the binary have neither the strong metallic features nor the deep water absorption bands indicates high effective temperatures of the objects. They both might be field-stars.

ITG 15A

The effective temperatures deduced from the UKIRT observations and that from the Subaru observations are very consistent with each other.

ITG 25 (IRAS 04370+2559)

While the UKIRT observations and the Subaru observations are consistent with each other in the strength of the 2.26 μm feature as well as the Q index, there is a discrepancy in the strength of the 2.21 μm feature, resulting in a different effective temperature. Because of higher signal-to-noise ratio in the Subaru observations than in the UKIRT observations, we use the effective temperature derived from the Subaru observations. For the Subaru observations, effective temperatures derived from the feature ratio and from the Q index are also different. As is the case of ITG 6, the veiling effect can easily increase the Q index, leading to a higher effective temperature. Because this object is an IRAS source indicating its young age, we believe the effective temperature derived from the feature ratio rather than that from the Q index.

For consistency between the effective temperature derived from the feature ratio and that from the Q index, the Q index should be 0.65, which means that 70% of the K -band luminosity is not of photospheric origin but from a circumstellar disk. If the same portion of the luminosity is due to the veiling for the companion ITG 25B, the Q index of the companion is suppressed to 0.08. This very low value indicates that effective temperature is less than 2700 K and the age is less than 1×10^6 yr, implying a low-mass brown dwarf.

ITG 33

te]cite.Martin00Martín(2000) ([cite]cite.Martin00Martín(2000)) classified the primary as a T Tauri star with spectral type of M3 and with A_v of 3.5 mag from optical spectroscopy. Spectral type derived from near-infrared spectroscopy is M0 or M4, consistent with the optical spectroscopy. Visual extinction is estimated to be 3.94 ± 0.55 from near-infrared photometry, also consistent with the optical spectroscopy. te]cite.Martin00Martín(2000) ([cite]cite.Martin00Martín(2000)) proposed an edge-on disk T Tauri star, like a companion

of HK Tau (000 [cite]cite.Koresko98Koresko(1998); 000 [cite]cite.Stapelfeldt98Stapelfeldt et al.(1998)). If so, visual extinction would be very large as much as 50 mag, like the HK Tau companion, inconsistent with A_v for ITG 33A. The location of ITG 33A is odd as a YSO in the HR diagram. Veiling effect may lead to high effective temperature. A spectrum with high signal-to-noise ratio is required to estimate effective temperature from metallic features.

te]cite.Martin00Martín(2000) ([cite]cite.Martin00Martín(2000)) also classified ITG 33B as a field-star from optical spectroscopy. However, their optical spectrum, as well as our near-infrared spectrum, are too noisy to classify this object as a field-star or a featureless YSO. Higher signal-to-noise ratio spectrum at optical and/or of near-infrared wavelength is required.

ITG 41 (IRAS 04385+2550)

This object is identified at optical wavelengths as Haro 6-34. Weak absorption features which may imply large amount of veiling prevents us from estimating the effective temperature, thus its mass and age.

ITG 45

te]cite.Martin00Martín(2000) ([cite]cite.Martin00Martín(2000)) found an H α absorption line in a spectrum of ITG 45A, indicating a field-star. Near-infrared spectrum of the primary contains Br γ absorption, also indicating a field-star. te]cite.Martin00Martín(2000) ([cite]cite.Martin00Martín(2000)) claims that the companion, ITG 45B, is also a field-star. However, the optical spectrum, as well as our near-infrared spectrum, is too noisy to classify it as a field-star or a YSO.

ITG 46

The location of ITG 46 in the HR diagram is unusual. Again a large amount of veiling may lead to high effective temperature. Otherwise, this object may be a field-star.

References

- [Aaronson et al.(1978)] Aaronson, M., Frogel, J. A., & Persson, S. E. 1978, ApJ, 220, 442
- [Ali et al.(1995)] Ali, B., Carr, J. S., DePoy, D. L., Frogel, J. A., & Sellgren, K. 1995, AJ, 110, 2415
- [Aspin et al.(1994)] Aspin, C., Sandell, G., & Russell, A. P. G. 1994, A&AS, 106, 165
- [Baraffe et al.(1998)] Baraffe, I., Chabrier, G., Allard, F., & Hauschildt, P. H. 1998, A&A, 337, 403
- [Barsony et al.(1997)] Barsony, M., Kenyon, S. J., Lada, E. A., (2000) Teuben, P. J. 1997, ApJS, 112, 109
- [Bertout et al.(1988)] Bertout, C., Basri, G., & Bouvier, J. 1988, ApJ, 330, 350
- [Bessell & Brett(1988)] Bessell, M., & Brett, J. 1988, PASP, 100, 1134
- [Bessell(1991)] Bessell, M. 1991, AJ, 101, 662
- [Briceño (1998)] Briceño, C., Hartmann, L., & Stauffer, J. 1998, AJ, 115, 2074
- [Comeron et al.(1993)] Comeron, F., Rieke, G., Burrows, A., & Rieke, M. 1993, ApJ, 416, 185

- [Cushing et al.(2000)] Cushing, M. C., Tokunaga, A. T., & Kobayashi, N. 2000, *AJ*, 119, 3019
- [D'Antona & Mazzitelli(1994)] D'Antona, F., & Mazzitelli, I. 1994, *ApJS*, 90, 467
- [D'Antona & Mazzitelli(1998)] D'Antona, F., & Mazzitelli, I. 1998, *Mem. Soc. Astron. Italiana*, 68, n.4
- [Dyck et al.(1998)] Dyck, H. M., van Belle, G. T., & Thompson, R. R. 1998 *ApJ*, 116, 981
- [Elias(1978)] Elias, J. 1978, *ApJ*, 224, 857
- [Fluks et al.(1994)] Fluks, M. A., Plez, B., The, P. S., de Winter, D., Westerlund, B. E., & Steenman, M. C. 1994, *A&AS*, 105, 311
- [Gomez et al.(1994)] Gomez, M., Kenyon, S., & Hartmann, L. 1994, *AJ*, 107, 1850
- [Greene & Meyer(1995)] Greene, T. P., & Meyer, M. R. 1995, *ApJ*, 450, 233
- [Greene & Lada(1997)] Greene, T. P., & Lada, C. J. 1997, *AJ*, 114, 2157
- [Gullbring et al.(1996)] Gullbring, E., Petrov, P. P., Ilyin, I., Gahm, G. F., & Lodén, K. 1996, *A&A*, 314, 835
- [Itoh et al.(1996)] Itoh, Y., Tamura, M., & Gatley, I. 1996, *ApJ*, 465, L129 (ITG)
- [Itoh et al.(1999)] Itoh, Y., Tamura, M., & Nakajima, T. 1999, *AJ*, 117, 1471
- [Jones et al.(1981)] Jones, T., Ashley, M., Hyland, A., & Ruelas-Mayoroga, A. 1981, *MNRAS*, 197, 413
- [Jones et al.(1994)] Jones, H. R. A., Longmore, A. J., Jameson, R. F., & Mountain, C. M. 1994, *MNRAS*, 267, 413
- [Kaifu et al.(2000)] Kaifu, N., Usuda, T. Hayashi, S. S. Itoh, Y. Akiyama, M. Yamashita, T. Nakajima, Y. & Tamura, M. et al. 2000, *PASJ*, 52, 1
- [Kenyon & Hartmann(1995)] Kenyon, S. J., & Hartmann, L. 1995, *ApJS*, 101, 117
- [Kim(1990)] Kim, C. Y. 1990, *Memories of the Faculty of Kyoto University*, Vol. 38, Series of Physics, Astrophysics and Chemistry, 1, 1
- [Kleinmann & Hall(1986)] Kleinmann, S. G., & Hall, D. N. B. 1986, *ApJS*, 62, 501
- [Koorneef(1983)] Koorneef, J. 1983, *A&A*, 128, 84
- [Kobayashi et al.(2000)] Kobayashi, N., Tokunaga, A. T., Terada, H., Goto, M., Weber, M., Potter, R., Onaka, P. M., Ching, G. K. et al. 2000, *Proc. SPIE*, 4008, 1056
- [Koresko(1998)] Koresko, C. D. 1998, *ApJ*, 507, L145
- [Lançon & Rocca-Volmerange(1992)] Lançon, A. & Rocca-Volmerange, B. 1992, *A&AS*, 96, 593
- [Leggett et al.(1996)] Leggett, S. K., Allard, F., Berriman, G., Dahm, C. C., & Hauschildt, P. H. 1996, *ApJS*, 104, 117
- [Lucas & Roche(2000)] Lucas, P. W., & Roche, P. F. 2000, *MNRAS*, 314, 858
- [Lucas et al.(2001)] Lucas, P. W., Roche, P. F., Allard, F. & Hauschildt, P. H. 2001, *MNRAS*, 326, 695
- [Luhman et al.(1997)] Luhman, K. L., Liebert, J., & Rieke, G. H. 1997, *ApJ*, 489, L165
- [Luhman & Rieke(1998)] Luhman, K. L., & Rieke, G. H. 1998, *ApJ*, 497, 354
- [Luhman et al.(1998)] Luhman, K. L., Rieke, G. H., Lada, C. J., & Lada, E. A. 1998, *ApJ*, 508, 347
- [Luhman(2000)] Luhman, K. L. 2000, *ApJ*, 544, 1044
- [Martín(2000)] Martín, E. L. 2000, *AJ*, 120, 2114
- [Martín et al.(2001)] Martín, E. L. Dougados, C., Magnier, E., Mnard, F., Cuillandre, J. C., Delfosse, X. 2001, *ApJ*, 561, L195
- [Meyer(1996)] Meyer, M. R. 1996, Ph. D. Thesis, University of Massachusetts
- [Meyer et al.(1997)] Meyer, M. R., Calvet, N. A., & Hillenbrand, L. A. 1997, *AJ*, 114, 288
- [Mountain et al.(1991)] Mountain, C. M., Robertson, D. J., Lee, T. J., & Wade, R. 1991, *Proc. SPIE*, 1235, 35
- [Najita et al.(1996)] Najita, J., Carr, J., & Tokunaga, A. T. 1996, *ApJ*, 456, 292
- [Oasa et al.(1999)] Oasa, Y., Tamura, M., & Sugitani, K. 1999, *ApJ*, 526, 336
- [Oasa et al.(2002)] Oasa, Y. et al. 2002, in preparation
- [Perrin et al.(1998)] Perrin, G., Coude du Foresto, V., Ridgway, S. T., Mariotti, J. M., Traub, W. A., Carleton, N. P., & Lacasse, M. G. 1998, *A&A*, 331 619
- [Ramirez et al.(1997)] Ramirez, S. V., DePoy, D. C., Frogel, J. A., Sellgren, K., & Blum, R. D. 1997, *AJ*, 113, 1411
- [Stapelfeldt et al.(1998)] Stapelfeldt, K., Krist, J. E., Ménard, F., Bouvier, J., Padgett, D. L., & Burrows, C.J. 1998, *ApJ*, 502, L65
- [Strom et al.(1988)] Strom, K. M., Strom, S. E., Edwards, S., Cabrit, S., & Strutskie, M. 1989, *AJ*, 97, 1451
- [Strom et al.(1993)] Strom, K. M., Strom, S. E., & Merrill, K. M. 1993, *ApJ*, 412, 233
- [Strom et al.(1995)] Strom, K. M., Kepner, J., & Strom, S. E. 1995, *ApJ*, 438, 813
- [Terndrup et al.(1991)] Terndrup, D. M., Frogel, J. A., & Whitford, A. E. 1991, *ApJ*, 378, 742
- [Tokunaga et al.(1998)] Tokunaga, A. T., Kobayashi, N., Bell J., Ching G. K., Hodapp, K. W., Hora, J. L., Neill, D., Onaka, P. M., et al. 1998, *Proc. SPIE*, 3354, 512
- [Tokunaga(2000)] Tokunaga, A. T. 2000 in *Astrophysical Quantities*, ed. A. N. Cox (Springer-Verlag), p. 143
- [Wichmann et al.(1998)] Wichmann, R., Bastian, U., Krautter, J., Jankovics, I., & Rucinski, S. M. 1998, *MNRAS*, 301, L39
- [Wilking et al.(1999)] Wilking, B. A., Greene, T. P., & Meyer, M. R. 1999, *AJ*, 117, 469